The Three-Dimensional Solution Structure of RANTES

Chun-wa Chung,[‡] Robert M. Cooke,*[,‡] Amanda E. I. Proudfoot,[§] and Timothy N. C. Wells[§]

Department of Biomolecular Structure, Glaxo Research and Development Ltd., Medicines Research Centre, Gunnels Wood Road, Stevenage, Hertfordshire, SG1 2NY, U.K., and Glaxo Institute for Molecular Biology, 14 Chemin des Aulx, 1228 Plan les Ouates, Geneva, Switzerland

Received March 22, 1995; Revised Manuscript Received May 10, 1995[⊗]

ABSTRACT: The solution structure of the chemokine RANTES (regulated on activation, normal T-cell expressed and secreted) has been determined using NMR spectroscopy. Backbone and side-chain ^1H and ^{15}N assignments have been obtained using a combination of two-dimensional homonuclear and three-dimensional heteronuclear spectra. Regular elements of secondary structure have been identified on the basis of a qualitative interpretation of NOE data, J(NH−Hα) coupling constants, and amide exchange rates. Three-dimensional structures were calculated from a total of 2146 experimental restraints using a combination of distance geometry and simulated annealing protocols. For the 13 best structures the average backbone (N, Cα, C) atomic rmsd from the mean coordinates for residues 5−65 is 0.64 Å (±0.14 Å) for the dimer and 0.50 Å (±0.08 Å) for the individual monomers. Each monomer consists of a three-stranded antiparallel β-sheet (residues 26−30, 38−43, 48−51) in a Greek key motif with a C-terminal helix (56−65) packed across the sheet, an arrangement similar to the monomeric structure of other members of this chemokine family (IL-8, PF4, MGSA/Groα, and MIP-1β). Overall, the RANTES dimer resembles that previously reported for MIP-1β.

RANTES[1] is an inflammatory cytokine that promotes the accumulation and activation of several types of leukocytes. The protein is highly basic (p*I* 9.5), with a molecular mass of 8 kDa, and is a member of the chemokine or interleukin 8 (IL-8) superfamily of proteins. Its distinctive pattern of adjacent cysteine residues near the N-terminus classifies it as one of the CC or β-subfamily of chemokines, which also includes MIP-1α, MIP-1β, and MCP-1,2,3. RANTES has been shown to be a chemoattractant for T-cells and monocytes *in vitro* and shows the ability to attract selectively $CD4^+/CD45RO^+$ T-cells while not attracting T-cells of other phenotypes (Schall *et al.*, 1990). This differential attraction implies that RANTES may be important in clinical situations such as asthma or allergen-induced late-phase skin reactions in atopic subjects (Baggiolini & Dahinden, 1994). This hypothesis is strengthened by the fact that RANTES is also a potent chemoattractant for eosinophils (Kameyoshi *et al.*, 1992; Alam *et al.*, 1993), which are strongly implicated in these diseases. A receptor that binds RANTES has recently been cloned from phorbol myristate acetate treated HL-60 (Gao *et al.*, 1993; Neote *et al.*, 1993) cells and has been shown to be one of the classical seven transmembrane spanning family of receptors.

Three-dimensional structures of four other human chemokines have been reported in the literature: IL-8 (Clore *et al.*, 1989, 1990; Baldwin *et al.*, 1991), PF4 (Zhang *et al.*, 1994), MIP-1β (Lodi *et al.*, 1994), and MGSA/Groα (Fairbrother *et al.*, 1994). The monomer structure in each case is very similar, being composed of a single C-terminal helix packed against a three-stranded antiparallel β-sheet by largely hydrophobic interactions. However, the aggregation state and oligomeric structures observed by NMR and X-ray can be very different: IL-8 and MGSA/Groα form compact dimers that extend the β-sheet structure and pack the two helices close together; PF4 exhibits a tetrameric structure with IL-8-type dimers being packed so that the extended β-sheets are back to back and slightly offset; MIP-1β is the only CC chemokine structure solved to date and forms a very different dimer, resembling a prolate ellipsoid in shape; most of the dimeric contacts occur between strands of β-sheet near the N-termini, resulting in an elongated molecule with a helix positioned at either end.

EXPERIMENTAL PROCEDURES

Sample Preparation. Recombinant human RANTES was expressed in *Escherichia coli* under the control of the T7 promoter expression system (Studier *et al.*, 1990) and purified using conventional procedures (A. E. I. Proudfoot and C. A. Power, unpublished). The protein was 98% pure as judged by reverse-phase HPLC analysis and was dialyzed extensively against 0.1% trifluoroacetic acid in water before lyophilization. NMR samples were prepared by resuspending the protein in a 50 mM sodium phosphate buffered solution made using either 99.9% D_2O or a 95% H_2O/5% D_2O mixture; the pH was then adjusted to 3.2 ± 0.1 (uncorrected meter reading) using NaOD or DCl. The resulting protein concentration ranged from 0.5 to 1.2 mM as estimated by UV absorption. Uniform ^{15}N labeling (98%)

‡ Glaxo Research and Development Ltd.
§ Glaxo Institute for Molecular Biology.
⊗ Abstract published in *Advance ACS Abstracts,* July 1, 1995.
[1] Abbreviations: RANTES, regulated upon activation, normal T-cell expressed and secreted; IL-8, interleukin 8; PF4, platelet factor 4; MGSA, melanoma growth simulating activity; GRO, growth-related gene product; NAP-2, neutrophil-activating peptide 2; MIP, macrophage inflammatory protein; MCP, monocyte chemoattractant protein; NMR, nuclear magnetic resonance; DQF-COSY, double-quantum-filtered correlated spectroscopy; NOESY, two-dimensional nuclear Overhauser enhancement spectroscopy; TOCSY, total correlation spectroscopy; TPPI, time-proportional phase incrementation; HSQC, heteronuclear single-quantum correlation; DG, distance geometry; SA, simulated annealing.

0006-2960/95/0434-9307$09.00/0

was performed using standard protocols (Reilly & Fairbrother, 1994; Bernard & Payton, 1995), and a single ^{15}N-labeled NMR sample was made with 50 mM sodium phosphate buffer in 95% H_2O/5% D_2O at pH 3.2 to give a protein concentration of 2 mM.

NMR Spectroscopy. All NMR spectra were recorded on a Bruker AMX600 spectrometer using an inverse probe equipped with a single shielded gradient coil. The majority of spectra were recorded at a temperature of 313 K; this temperature was found to be a good compromise between spectral quality and sample stability. In addition, some experiments were also recorded at 298 K. A spectral width of 16 ppm in the ^1H and 60 ppm in the ^{15}N dimensions was used unless specified. ^{15}N shifts were indirectly referenced to ammonia (Live *et al.*, 1984; Bax & Subramanian, 1986) using an aqueous solution of acetanilide (Witanowski *et al.*, 1993). Proton chemical shifts were referenced with respect to dioxane at 3.75 ppm.

Two-dimensional DQF-COSY (Piantini *et al.*, 1982), NOESY (Jeener *et al.*, 1979; Kumar *et al.*, 1980), and TOCSY (Braunschweiler & Ernst, 1983; Bax & Davis, 1985) spectra were recorded with 2048 complex points in t_2 and 512 increments in t_1. Quadrature detection in F_1 was achieved with the TPPI procedure (Drobny *et al.*, 1979; Bodenhausen *et al.*, 1980). Data were subsequently processed and zero-filled to give square spectra of dimensions 2048 by 2048. The mixing times in the NOESY experiments ranged from 100 to 200 ms; no zero-quantum suppression was performed. The TOCSY spectra were all z-filtered (Rance, 1987; Bazzo & Campbell, 1988) using between 36 and 65 ms of DIPSI-2 (Shaka *et al.*, 1988; Rucker & Shaka, 1989) as the isotropic mixing sequence. Variation of the delays bracketing the mixing sequence within each increment was used to eliminate zero-quantum contributions (Macura *et al.*, 1981; Sørensen *et al.*, 1984). Double-quantum spectra (Bodenhausen *et al.*, 1984) were acquired with 2048 complex points in t_2 and 1024 increments in t_1, with spectral widths of 16 and 28 ppm, respectively; a 10 ms delay was used to optimize the generation of double-quantum (DQ) coherence. TPPI was also used for quadrature detection in this case, and DQ spectra were again processed to give square spectra of 2048 by 2048 points by zero-filling. Water suppression in all these two-dimension experiments was achieved using 1−1.3 s of low-power presaturation with the ^1H carrier placed at the water frequency and a relaxation delay of 1 s. Additional postacquisition suppression of the residual water signal was achieved by convolution of the time domain data using the method of Marion *et al.* (1989a).

Three-dimensional heteronuclear separated NOESY-HSQC and TOCSY-HSQC spectra (Marion *et al.*, 1989b,c; Fesik & Zuiderweg, 1990) were acquired with 128 (t_1) by 32 (t_2) by 512 (t_3) complex points with spectral widths of 14 ppm (F_1 ^1H), 60 ppm (F_2 ^{15}N), and 8 ppm (F_3 ^1H) in the respective dimensions. The spectra were recorded in the pure absorption mode using States−TPPI (States *et al.*, 1982; Marion *et al.*, 1989d) for quadrature detection in t_1 and t_2 and simultaneous acquisition in t_3. Zero-filling and linear prediction then produced processed spectra of 512 (F_1) by 64 (F_2) by 1024 (F_3) points. As a modified form of WATERGATE was implemented for water suppression (Sklenár *et al.*, 1993) in these 3D experiments, the ^1H carrier frequency was set to the center of the amide region, and a significant reduction in the spectral width in F_3 was permitted. A mixing time of 150 ms was used for the NOESY-HSQC spectrum, and one of 49 ms was used for the *z*-filtered TOCSY-HSQC spectrum.

$^3J(NH-H\alpha)$ coupling constants were measured by the method of Stonehouse and Keeler (1995) using cross sections taken from a 2D $^{15}N-^1H$ HSQC spectrum. Amide protons protected from exchange with solvent were defined from those whose resonances show at least one remaining cross-peak in a 10 h TOCSY experiment of a sample 2 h after dissolution in D_2O at pH 3.2 at 313 K. A similar spectrum, recorded after 60 h exposure to D_2O, allowed some to be classified as highly protected.

All NMR data were processed on a Silicon Graphics Indigo-2 Workstation using FELIX (BIOSYM Technologies, Inc., San Diego).

Structure Calculation. Interproton distance restraints were derived from NOEs assigned in the 2D homonuclear and 3D heteronuclear-separated NOESY spectra acquired with mixing times of 150 ms. The assigned NOEs were classified as strong, medium, and weak and allocated distance restraints of 1.0−3.0, 2.0−4.0, and 2.0−5.0 Å, respectively. In addition, where appropriate, lower bounds between nonbonded protons were set to the sum of their van der Waals radii. Upper limits for distances involving methyl protons or nonstereospecifically assigned methylene protons were corrected for center averaging (Wüthrich *et al.*, 1983).

To allow for motional averaging, only coupling constants outside the range 5.5−8.5 Hz were converted, initially, into contiguous ranges of torsion angle constraints for distance geometry and then into multiple ranges (up to four) for the later stages of structure refinement. The Karplus equation with the constants $A = 6.7$, $B = -1.3$ and $C = 1.5$ (Pardi *et al.*, 1984; BIOSYM NMRArchitect Manual, 1994) was used to convert the $^3J(HN-H\alpha)$ couplings into ϕ angles with an error margin of ±20°. Hydrogen bond restraints were only added in the final stages of refinement in cases where both donor and acceptor atoms could be unambiguously identified from evidence of slow amide proton−solvent exchange and predicted secondary structure. Two distance restraints, $r(H-O) = 1.7-2.3$ Å and $r(N-O) = 2.5-3.4$ Å, were used to define each hydrogen bond.

Structures were generated using a hybrid distance geometry−dynamical simulated annealing protocol based on the method of Nilges *et al.* (1988). Initial distance geometry structures (Havel & Wüthrich, 1984; Havel, 1991) were calculated using the program DG-II (BIOSYM Technologies, Inc., San Diego) and regularized and minimized using DISCOVER (BIOSYM Technologies, Inc., San Diego). Acceptable structures were then subjected to a dynamical simulated annealing procedure within X-PLOR 3.1 (Brünger, 1992). Adopting the strategy of Nilges (1993) additional symmetry restraints, namely, noncrystallographic symmetry restraints and symmetrical distance restraints, were incorporated into this final stage of refinement to ensure the generation of a symmetrical dimer. Calculations were performed on Silicon Graphics computers.

RESULTS AND DISCUSSION

Resonance Assignment. Initial experiments were directed at finding the optimum conditions for NMR studies. The samples were found to be reasonably soluble and stable at pH 3.2 at 313 K and could be used over a time period of

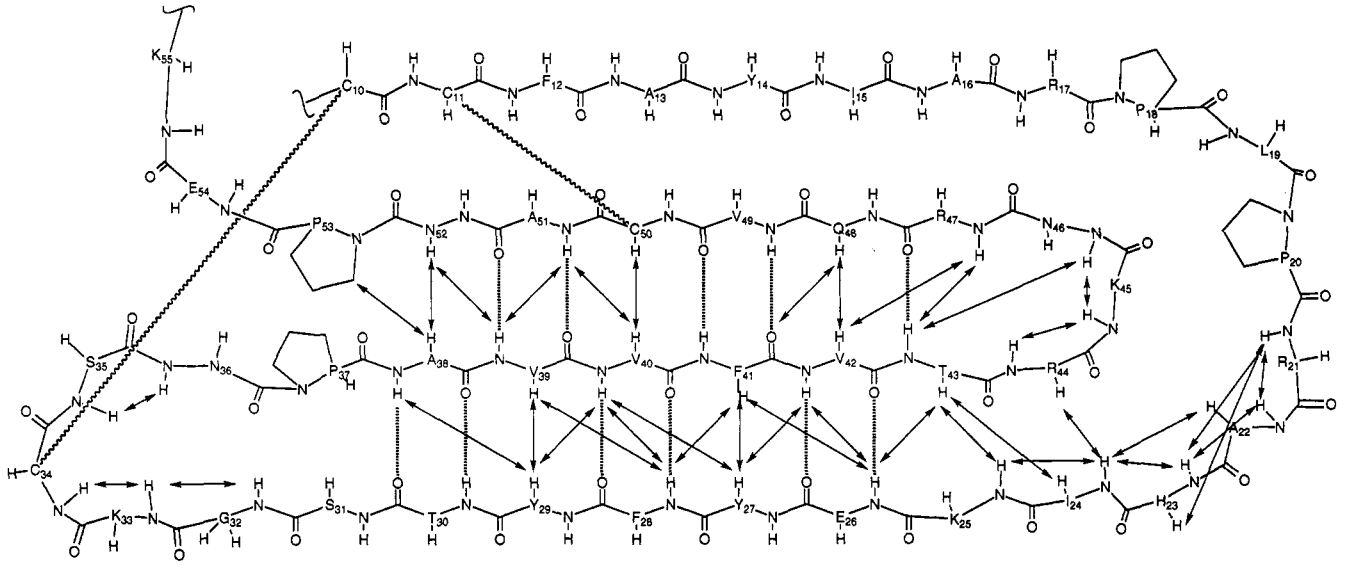

FIGURE 1: Schematic representation of the antiparallel β-sheet structure of RANTES as determined by qualitative NOE connectivities, J(NH−Hα) coupling constants, and amide proton exchange rates. Observed interstrand NOEs are indicated by arrows, and hydrogen bonds predicted by experimental data and initial structures generated in the absence of hydrogen bond constraints are indicated by thick broken lines. The two disulfide bridges are shown in wavy lines between Cys 10 and Cys 34 and Cys 11 and Cys 50, respectively.

months with no significant evidence of degradation. Resonance assignments were carried out using the well-established protocols (Wüthrich, 1986; Clore & Gronenborn, 1987). Spin systems were initially identified by their characteristic patterns in DQF-COSY, NOESY, and TOCSY spectra, although the TOCSY spectra were consistently of lower quality than was expected for a protein of this size. Most assignments were performed using spectra recorded at 313 K, but TOCSY spectra at 298 K were used to trace back from the ϵNH resonances of some lysine residues. The double-quantum spectrum from the D_2O sample was essential in fully assigning the aromatic portions of the Phe residues, thereby allowing the aromatic spin systems to be connected to the aliphatic portion of the same residue. Otherwise this was often ambiguous, presumably due to the close packing of aromatic residues. The side-chain NH resonances of four Asn residues and a single Gln residue are not fully resolved in the ^{1}H spectra but can be resolved in a 2-D ^{15}N−^{1}H HSQC spectrum and linked with β- or γCH resonances by NOEs using the heteronuclear 3D spectra. The increased resolution of a third dimension was also extremely useful for unambiguous identification of NOEs between NH resonances close to the diagonal and for progressing assignments through crowded regions of the proton spectrum. The heteronuclear spectra also confirmed that the resonance at 5.3 ppm arises from an NH and allowed its assignment to Leu 19.

A list of assignments at a temperature of 313K and pH 4.5 is given in Table S1 of the supporting information. The ^3J(NH−Hα) coupling constants measured from the 2D ^{15}N−^{1}H HSQC spectrum and the 25 backbone amide protons which exchange slowly with solvent are also listed in Table S1 of the supporting information. Upon combining this information with a qualitative interpretation of the sequential NOE data, the following elements of secondary structure can be located: three strands of a β-sheet encompassing residues 26−30, 38−43, and 48−51 and a C-terminal helix (residues 56−65). Consideration of nonsequential NOEs involving the backbone resonances of these residues allows determination of the β-sheet arrangement as shown schematically in Figure 1. This is consistent with the observed patterns of slow amide proton exchange. The peptide bonds for the proline residues P9, P18, P37, and P53 are all in the *trans* conformation as confirmed by strong Hα(i − 1) to Hδ(Pro + i) sequential NOEs (NOEs from S1:Hα to P2:Hδ and L19: Hα to P20:Hδ could not be unambiguously identified).

Three-Dimensional Structure Generation. Three-dimensional structures were initially generated assuming that RANTES was a monomer at the concentrations used. Analysis of these initial structures identified several NOEs which could not arise from a monomer. Combined with the knowledge that other chemokines are dimers at millimolar concentrations and that gel filtration experiments indicate that RANTES exists as a dimer at higher concentrations (Paolini *et al.*, 1994; A. E. I. Proudfoot, unpublished), subsequent structures were produced as dimers. A total of 2146 NOE-derived distance constraints were identified for the dimer. These consisted of 808 intraresidue constraints, 522 sequential constraints, 158 medium-range constraints (58 i, i + 2; 72 i, i + 3; 28 i, i + 4), and 658 longer range constraints. Most NOEs were assigned on the basis of sequential assignments alone, but a small number were identified from examination of the initial 3D structures and reexamination of spectra. Fifty intermonomer NOEs were only incorporated after trial structures confirmed they could not arise from within one monomer. For V58 and V39 the γCH$_3$ resonances display markedly different NOEs, and these were stereospecifically assigned on the basis of trial structures; the δCH$_3$ resonances of L19 and L65 were stereospecifically assigned on the same basis. The NOEs used for the final structure generation are summarized in the contact diagram of Figure 2. In addition, 42 hydrogen bonds per dimer were identified from the slow amide proton exchange data, the secondary structure topology, and initial structures generated in the absence of H-bond data. All but two of these correspond to regions of regular secondary structure within the monomer; the remainder occur across the dimer interface. Restraints for 86 ϕ torsion angles were derived from the NH−αCH coupling constants.

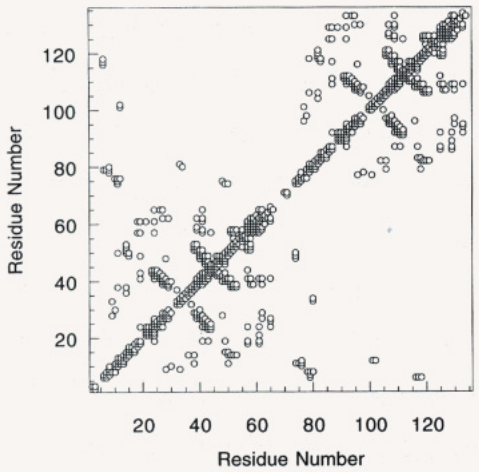

FIGURE 2: NOEs observed for the RANTES dimer. For the purposes of this plot the residues of the dimer have been numbered contiguously from 1−68 for one monomer and 69−136 for the other. The elements of secondary structure are readily apparent: β-sheet as rows of contacts perpendicular to the diagonal; helices as a thickening of the diagonal. Intermonomer contacts are seen in the top left and bottom right areas of the diagram.

Table 1: Structural Statistics for 13 Refined RANTES Structures[a]

experimental distance restraints	
NOE (2146)+ H-bond (84)[b]	
av restraint violation (Å)	0.049 ± 0.006
av no. of restraint violations >0.5 Å per structure	0.92 ± 1.26
av no. of restraint violations >0.2 Å per structure	40.8 ± 9.4
av no. of restraint violations >0.1 Å per structure	84.1 ± 12.0
average deviations from idealized covalent	
bonds (Å)	0.0065 ± 0.0006
angles (Å)	0.87 ± 0.04
improper torsions (deg)	3.2 ± 0.1
deviation from ideal symmetric dimer	
av of all atoms rmsd between monomers (Å)	0.39 ± 0.03
average rmsd from mean structure	
backbone atoms (N, Cα, C) (Å)	0.50 ± 0.08,[c] 0.64 ± 0.14[d]
all heavy atoms (Å)	1.01 ± 0.07,[c] 1.11 ± 0.12[d]

[a] Values quoted are mean ± standard deviation. [b] None of the 13 final structures exhibited NOE restraint violations of >1.0 Å or H-bond restraint violations of >0.2 Å. [c] For monomer (5−65). [d] For dimer (5−65, 5′−65′).

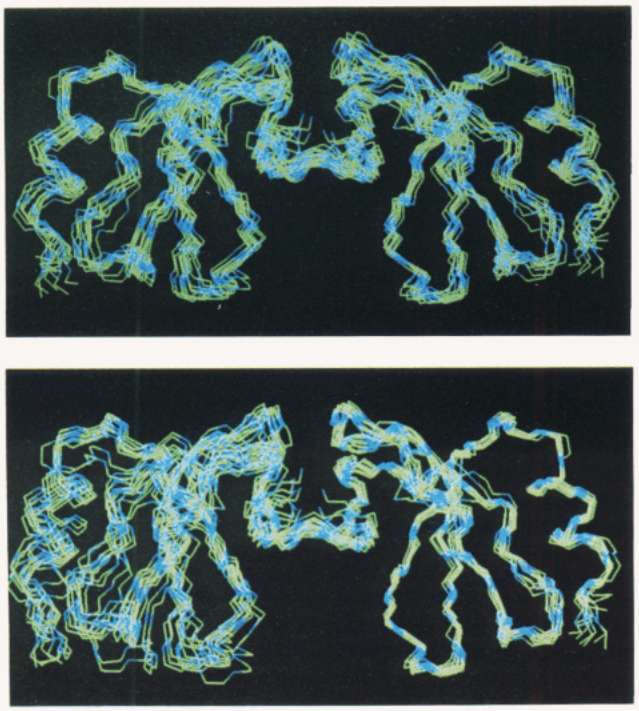

FIGURE 3: Best-fit superposition of the backbone atoms (N, Cα, C) of 13 structures of RANTES. In (A, top) residues 5−65 and 5′−65′ from both halves of the dimer were used for the superposition; in (B, bottom) only residues 5−65 from the right-hand monomer were used.

Structures created by distance geometry were assessed on the grounds of energy, restraint violations, and deviation from standard protein geometries. Approximately 45% of the structures could be classified as belonging to a low-energy family. The remainder displayed energies typically four to ten times higher than the first family and were discarded. The low-energy structures were submitted to a simulated annealing protocol. Following this, the 13 best structures were analyzed. An overlay of the backbone atoms of these 13 structures is shown in Figure 3. The convergence and restraint violations of the final structures are summarized in Table 1.

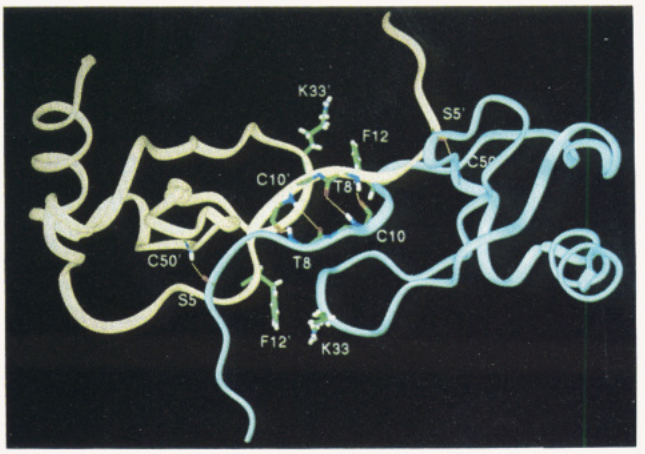

FIGURE 4: RANTES dimer interface. The backbone of each monomer is depicted by a differently colored ribbon. At the center of the dimer, a small segment of antiparallel β-sheet is formed by residues 8−10 and 10′−8′; the backbone atoms of these residues are shown in solid. Intermonomer hydrogen bonds exist between Cys 50 and Ser 5′ and Ser 5 and Cys 50′; the relevant carbonyl and amide protons of these residues are highlighted. The side chain of Lys 33 and the ring of Phe 12′ (and 12 and 33′) are also in contact and are displayed.

Description of the Structure. The RANTES dimer resembles a prolate ellipsoid where each monomer is superimposable (within experimental error). Each monomer folds to form a three-stranded β-sheet arranged in a Greek key motif, with an N-terminal extended region and a C-terminal helix lying on one face of the sheet. The N-terminus appears to be disordered before residue 5. Residues 8−10 adopt a β-strand conformation, paired with the corresponding residues across the dimer interface. Two disulfide bonds pair Cys 10 with Cys 34 and Cys 11 with Cys 50. Residues 12−16 adopt an extended conformation near the edge of the face of the β-sheet leading to a broad turn involving residues 17−23 that runs almost parallel to the C-terminal helix. The first strand of the β-sheet encompassing residues Ile 24 to Thr 30 then follows. This is somewhat distorted from ideal conformations, leading to smaller than expected ^3J(NH−Hα) coupling constants, and although the amide protons of Tyr

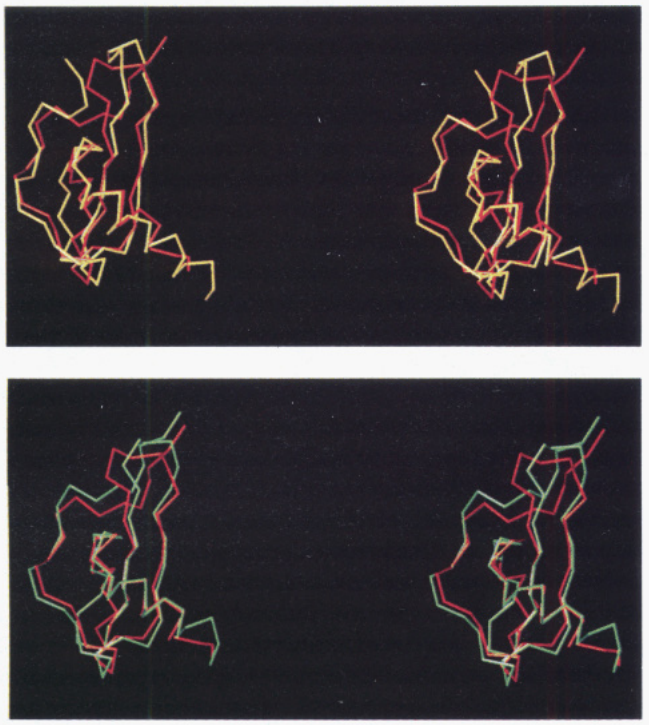

FIGURE 5: Superposition of the nonminimized average backbone of the RANTES monomer (red) with that of (A, top) IL-8 (yellow) and (B, bottom) MIP-1β (green) (Brookhaven entries are 1il8.pdb, and 1hum.pdb respectively). Structures were superimposed on the basis of topologically equivalent residues.

27 and Tyr 29 are protected from exchange, this does not appear to arise from hydrogen bonds across the β-sheet. Rather, they appear to be shielded by the side chains of Glu 26 and Tyr 27, respectively. Another broad turn from Ser 31 to Pro 37 contains one end of the first disulfide bond and leads into the second strand of the sheet. This runs from Ala 38 to Thr 43 and is hydrogen bonded on both sides to the first and third strands. A smaller turn from residue 43 to residue 47 connects the second strand to the third, which runs from Gln 48 to Ala 51. A particularly stable core to the β-sheet is apparent from the protection against exchange over 60 h observed for the amide protons of residues 28, 39, 40, and 49. Residues 52−55 take the chain out of the plane of the sheet and connect to the helix (residues 56−65). The helix packs diagonally against one face of the sheet with residue Trp 57 near Leu 19, Pro 18, and Phe 41 and Leu 65 near Ile 24 and Glu 26.

The dimer interface (Figure 4) is defined by 50 NOEs and four hydrogen bonds and may be viewed as centered on a short section of antiparallel β-sheet pairing residues 8−10 of one monomer with residues 10′−8′ of the other. A 2-fold rotation axis sits between each Pro 9 residue. Hydrogen bonds exist between the NH of Cys 10 from each monomer to the backbone carbonyl of Thr 8 in the other monomer and between the NH of Cys 50 and the backbone carbonyl of Ser 5. On each edge of the interface contact is made between Phe 12 of one subunit and Lys 33 of the other, producing upfield shifts for the Lys resonances. Val 49 and Cys 50 from each monomer contact Asp 6 and Ser 5 from the other, with a hydrogen bond from Cys 50 NH to Ser 5 CO. The position of each monomer with respect to the other is slightly disordered, as is apparent from the better fit of the structures obtained when the monomers are superimposed individually (Figure 3B). It is not clear whether this reflects true mobility at the interface. While the area of the dimer interface for the 13 structures is 1331 ± 75 Å^2, its elongated shape would allow hinge movement about an axis perpendicular to the symmetry axis without significant violations of the 25 intersubunit NOEs per monomer. The fact that widespread protection from exchange of amide protons at the interface is not observed indicates the dimeric structure is not absolutely maintained.

Comparison with Other Chemokines. Clearly the topology of the RANTES monomer is very similar to that of the previously reported chemokines (Figure 5). Some differences are imposed due to the insertions and deletions of amino acids between the CXC and CC classes of chemokines, but each maintains a three-stranded β-sheet bordered on one face by a helix, and some well-conserved features of the structure are apparent from the similarities in chemicals shifts between RANTES and IL-8. For example, the resonance shifts for Val 58, Leu 19, and Pro 18 of RANTES are diagnostic of a spatial relationship between these residues and Trp 57, similar to that in IL-8. Significant differences are observed between the helices in RANTES and IL-8 and MGSA/Groα. The deformation found in the first strand of

```
                  1         10        20        30        40        50        60        70
CC Chemokines     :         :         :         :         :         :         :         :
RANTES      -SPYSSDT-TPC-CFAYIARPLPRAHIKEYFYTSGK--CSNPAVVFVTRK-NRQVCANPEKKWVREYINSLEMS
MIP-1A      -ASLAADTPTAC-CFSYTSRQIPQNFIADYFETSSQ--CSKPGVIFLTKR-SRQVCADPSEEWVQKYVSDLELSA
LD78B       -APLAADTPTAC-CFSYTSRQIPQNFIADYFETSSQ--CSKPSVIFLTKR-GRQVCADPSEEWVQKYVSDLELSA
MIP-1B      -APMGSDPPTAC-CFSYTARKLPRNFVVDYYETSSL--CSQPAVVFQTKR-SKQVCADPSESWVQEYVYDLELN
G26         SAPMGSDPPTAC-CFSYTARKLPRNFVVDYYETSIL--CSQPAVVFQTKR-SKQVCADPSETWVQEYVYDLELN
MCP-1       -QPDAINAPVTC-CYNFTNRKISVQRLASYRRITSSK-CPKEAVIFKTIV-AKEICADPKQKWVQDSMDHLDKQTQTP
MCP-2       AQPDSVSIPITC-CFNVINRKIPIQRLESYTRITNIQ-CPKEAVIFKTKR-GKEVCADPKERWVRDSMKHLDQIFQNL
MCP-3       -QPVGINTSTTC-CYRFIN-KIPKQRLESYRRTTSSH-CPREAVIFKTKL-DKEICADPTQKWVQDFMKHLDKKTQTPKL
I309        --KSMQVPFSRC-CFSFAEQEIPLRAILCYRNTSSI--CSNEGLIFKLKR-GKEACALDTVGWVQRHRKMLRHCPSKRK
CXC Chemokines
MIP2A       ---APLATELRCQCLQTLQG-IHLKNIQSVKVKSPGPHCAQTEVIATLKN-GQKACLNPASPMVKKIIEKMLKNGKSN
MIP2B       ---ASVVTELRCQCLQTLQG-IHLKNIQSVNVRSPGPHCAQTEVIATLKN-GKKACLNPASPMVQKIIEKILNKGSTN
PBP         -LDSDLYAELRCMCIKTTSG-IHPKNIQSLEVIGKGTHCNQVEVIATLKD-GRKICLDPDAPRIKKIVQKKLAGDESAD
IL-8        AVLPRSAKELRCQCIKTYSKPFHPKFIKELRVIESGPHCANTEIIVKLSD-GRELCLDPKENWVQRVVEKFLKRAENS
PF4         ------DGDLQCLCVKTTSQ-VRPRHITSLEVIKAGPHCPTAQLIATLKN-GRKICLDLQAPLYKKIIKKLLES
GRO         ---ASVATELRCQCLQTLQG-IHPKNIQSVNVKSPGPHCAQTEVIATLKN-GRKACLNPASPIVKKIIEKMLNSDKSN
GCP         -PVSAVLTELRCTCLRVTLR-VNPKTIGKLQVFPAGPQCSKVEVVASLKN-GKQVCLDPEAPFLKKVIQKILDSGNK
INIG        IQGVPLSRTVRCTCISISNQPVNPRSLEKLEIIPASQFCPRVEIIATMKKKGEKRCLNPESKAIKNLLKAVSKEMSKRSP
PF4-variant --EAEEDGDLQCLCVKTTSQ-VRPRHITSLEVIKAGPHCPTAQLIATLKN-GRKICLDLQALLYKKIIKEHLES
```

FIGURE 6: Sequences of CC and CXC chemokines aligned on the basis of residue conservation and 3D structural similarity. The numbering found at the top of the alignment table relates to that of RANTES.

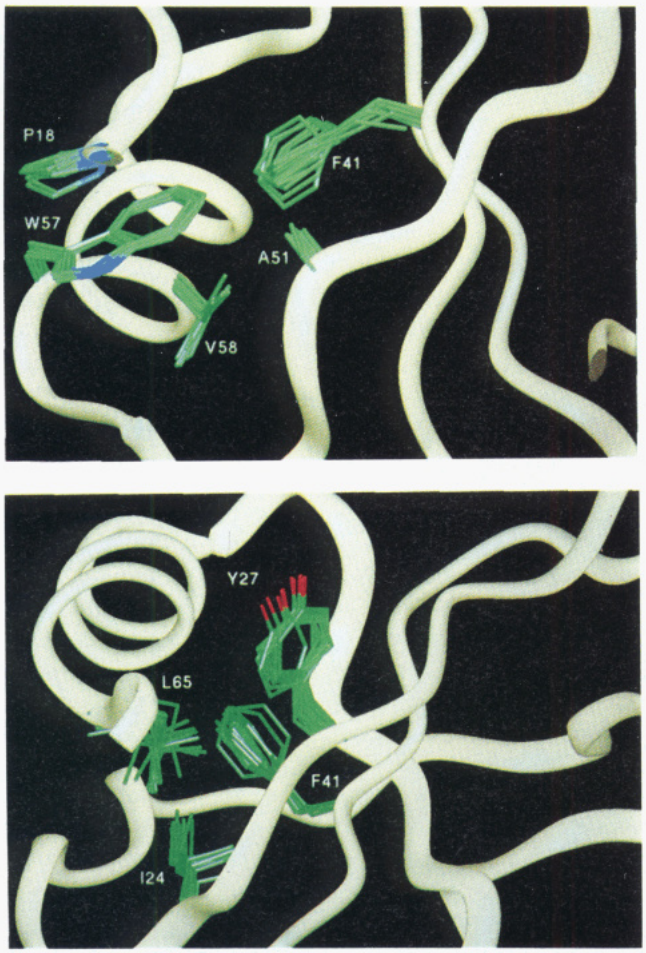

FIGURE 7: Two regions of hydrophobic interactions defining the relative orientation of the C-terminal helix with respect to the underlying β-sheet: (A, top) the start of the helix; (B, bottom) the end of the helix.

the β-sheet of RANTES is not observed in IL-8 or MGSA/Groα, but with the latter pair this strand forms the dimer interface, which may help maintain its regular geometry. The helix is shorter in RANTES and aligned slightly differently with respect to the sheet. The end of the helix of RANTES (after approximately residue 65) appears to be frayed, as in MGSA/Groα, but unlike the situation for IL-8.

Using the structures of RANTES and IL-8, it is possible to produce an aligned set of chemokine sequences based on three-dimensional similarity (Figure 6). In all reported chemokine sequences only the four cysteine residues are totally conserved. In addition, highly conserved substitutions are found at Phe 12, Leu 19, Ile 24, Val 39, and Val 40 (RANTES nomenclature). These residues are located on or around the β-sheet, but the interface between the helix and the sheet does not appear to be well conserved. The predicted amino acid sequences of the nine distinct human CC chemokines (Figure 6) show that several additional amino acids are absolutely maintained. These are Tyr 27, Phe 41, Ala 51, Trp 57, Val 58, and Leu 65, all of which have a role in maintaining the relative orientation of the helix to the sheet. At one end of the helix there is close packing of the hydrophobic residues Pro 18, Ala 51, Phe 41, Trp 57, and Val 58 (Figure 7A) whereas at the other end residues Ile 24, Phe 41, Leu 65, and Tyr 27 are in contact (Figure 7B). In RANTES the aromatic residue Phe 12 plays a structural role in the orientation of the loop between strands two and three

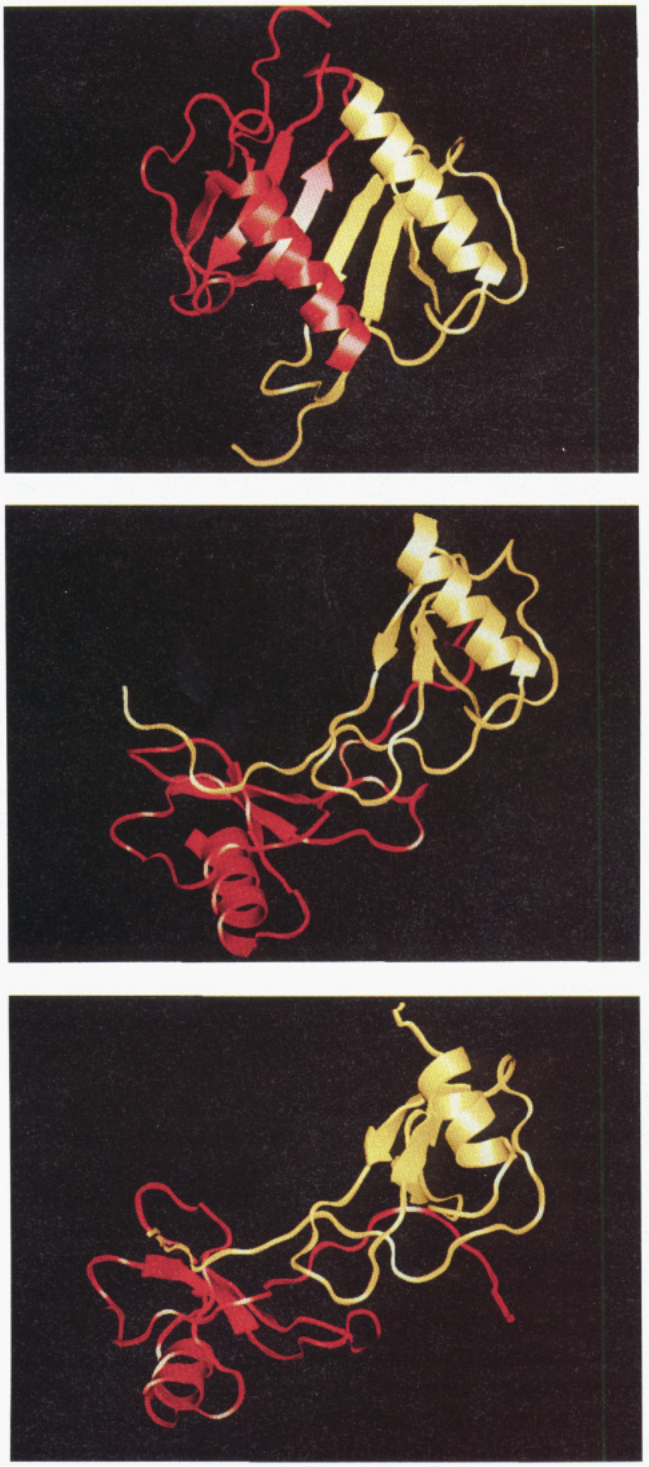

FIGURE 8: Dimeric structures of (A, top) IL-8, (B, middle) MIP-1β, and (C, bottom) RANTES shown as protein cartoons using QUANTA 4.0 (Molecular Simulations, Inc.). Each monomer is colored differently for clarity.

of one monomer with the N-terminal portion of the other monomer (Figure 4C). This interaction is hydrophobic in nature and involves the packing of the Phe aromatic ring against the aliphatic side chain of Lys 33, resulting in large shifts for resonances of the lysine. The WV motif within CC chemokines marks a tight turn at the start of the helix and produces highly characteristic shifts for Val 58, which may be diagnostic of this structure.

Two types of dimers have been reported for this family of proteins (Clore & Gronenborn, 1995), the compact dimer of IL-8 (Figure 8A) and the elongated ellipsoid structure of

MIP-1β (Figure 8B), and RANTES (Figure 8C) bears close resemblance to the latter. Lodi *et al.* (1994) hypothesized that the change in the dimeric structure between IL-8 and MIP-1β could be rationalized by a shorter helix in the latter, which allows fewer intermonomer contacts to be formed, and specific sequence differences such that the ellipsoidal dimer of MIP-1β relieved repulsion between like charges and allowed greater burial of hydrophobic residues (Clore & Gronenborn, 1995). The relevant sequence differences are generally maintained between the CC and the CXC chemokines, and given that MGSA/Groα resembles IL-8 and RANTES resembles MIP-1β, the division in dimer arrangement may be absolute. The cellular targets differ between the two branches of the chemokine family, but it is unclear whether this is determined by the difference in dimer structure. Although it is interesting to note that the residues of IL-8 implicated in receptor binding would be involved in a RANTES-like dimer interface, it is uncertain whether the chemokines act as monomers or dimers at their receptors (Herbert *et al.*, 1991; Moser *et al.*, 1993; Gayle *et al.*, 1993; Clark-Lewis *et al.*, 1991; Clubb *et al.*, 1994). Rajarthnam *et al.* (1994) demonstrated that a monomeric form of IL-8 is still fully active in neutrophil activation, and several groups (Burrows *et al.*, 1994; Paolini *et al.*, 1994) have shown that IL-8 is a monomer at physiological concentrations. However, there is indication that the chemokines act in an immobilized form bound to the endothelial surface where the local concentration may support a dimeric state (Tanaka *et al.*, 1993). Thus while the cell-type specificity of each class of chemokines must be determined by their amino acid sequences, it is more likely that these are manifested via receptor−ligand contacts rather than through the quaternary structure of the ligand (Lusti-Narasimhan *et al.*, 1995).

CONCLUSIONS

The CC chemokine RANTES forms a dimer in solution. While the RANTES monomer displays a topology similar to that of the other members of the chemokine family, differences do exist, notably concerning the length and location of the C-terminal helix. The disposition of the monomers within the dimer, however, resembles the extended ellipsoid of MIP-1β, rather than the compact dimer of IL-8 and MGSA/Groα, suggesting that these topologies may be specific to each subclass of the chemokine family. A detailed understanding of the relationship between the tertiary and quaternary structures of the chemokines and their activities will require an extensive mutagenesis program.

ACKNOWLEDGMENT

We thank Dr. Christine Power and Dr. Bernard Allet for molecular biology support, Dr. Alain Bernard, Ferderic Borlat, and Marc-Oliver Montjovent for protein production, purification, and characterization, and Dr. Jon Stonehouse for the use of his program to measure coupling constants.

SUPPORTING INFORMATION AVAILABLE

Table S1 giving ^{1}H and ^{15}N NMR assignments for RANTES at 313 K, pH 3.2 (2 pages). Ordering information is given on any current masthead page.

REFERENCES

Alam, R., Stafford, S., Forsythe, P., Harrison, R., Faubion, D., Lett-Brown, M. A., & Grant, J. A. (1993) *J. Immunol. 150*, 3443−3447.

Baggiolini, M., & Dahinden, C. A. (1994) *Immunol. Today 15*, 127−133.

Baldwin, E. T., Weber, I. T., St. Charles, R., Xuan, J.-C., Appella, E., Yamada, M., Matsushima, K., Edwards, B. F. P., Clore, G. M., Gronenborn, A. M., & Wlodawer, A. (1991) *Proc. Natl. Acad. Sci. U.S.A. 88*, 502−506.

Bax, A., & Davis, D. G. (1985) *J. Magn. Reson. 65*, 355−360.

Bax, A., & Subramanian, S. (1986) *J. Magn. Reson. 67*, 565−569.

Bazzo, R., & Campbell, I. D. (1988) *J. Magn. Reson. 76*, 358−361.

Bernard, A. R., & Payton, M. A. (1995) *Current Protocols for Protein Science*, John Wiley & Sons, New York (in press).

Bodenhausen, G., Vold, R. L., & Vold, R. R. (1980) *J. Magn. Reson. 37*, 93−106.

Bodenhausen, G., Kogler, H., & Ernst, R. R. (1984) *J. Magn. Reson. 58*, 370−388.

Braunschweiler, L., & Ernst, R. R. (1983) *J. Magn. Reson. 53*, 521−528.

Brünger, A. T. (1992) *X-PLOR (version 3.1) Manual*, Yale University Press, New Haven, CT.

Burrows, S. D., Doyle, M. L., Murphy, K. P., Franklin, S. G., White, J. R., Brooks, I, McNulty, D. E., Scott, M. O., Knutson, J. R., Porter, D., Young, P. R., & Hensley, P. (1994) *Biochemistry 33*, 12741−12745.

Clark-Lewis, I., Schumacher, C., Baggiolini, M., & Moser, B. (1991) *J. Biol. Chem. 266*, 23128−23134.

Clore, G. M., & Gronenborn, A. M. (1987) *Protein Eng. 1*, 275−288.

Clore, G. M., & Gronenborn, A. M. (1995) *FASEB J. 9*, 57−62.

Clore, G. M., Appella, E., Yamada, M., Matsushima, K., & Gronenborn, A. M. (1989) *J. Biol. Chem. 264*, 18907−18911.

Clore, M. G., Appella, E., Yamada, M., Matsushima, K., & Gronenborn, A. M. (1990) *Biochemisty 29*, 1689−1696.

Clubb, R. T., Omichinski, J. G., Clore, G. M., & Gronenborn, A. M. (1994) *FEBS Lett. 338*, 93−97.

Drobny, G., Pines, A., Sinton, S., Weitkamp, D. P., & Wemmer, D. (1979) *Faraday Symp. Chem. Soc. 13*, 49−55.

Fairbrother, W. J., Reilly, D., Colby, T., Hesselgesser, J., & Horuk, R. H. (1994) *J. Mol. Biol. 242*, 252−270.

Fesik, S. W., & Zuiderweg, E. R. P. (1990) *Q. Rev. Biophys. 23*, 97−131.

Gao, J.-L., Kuhns, D. B., Tiffany, H. L., McDermot, D., Li, X., Francke, U., & Murphy, P. M. (1993) *J. Exp. Med. 177*, 1421−1427.

Gayle, R. B., III, Sleuth, P. R., Birks, C. W., Weerawarna, K. S., Ceretti, D. P., Kozlosky, C. J., Nelson, N., Vanden Bos, T., & Beckmann, M. P. (1993) *J. Biol. Chem. 268*, 7283−7289.

Havel, T., & Wüthrich, K. (1984) *Bull. Math. Biol. 46*, 673−698.

Havel, T. F. (1991) *Prog. Biophys. Mol. Biol. 56*, 43−78.

Herbert, C. A., Vitangcol, R. V., & Baker, J. B. (1991) *J. Biol. Chem. 266*, 18989−18994.

Jeener, J., Meier, B. H., Bachmann, P., & Ernst, R. R. (1979) *J. Chem. Phys. 71*, 4546−4553.

Kameyoshi, Y., Dorschner, A., Mallet, A. I., Christophers, E., & Schroder, J. M. (1992) *J. Exp. Med. 176*, 586−592.

Kumar, A., Ernst, R. R., & Wüthrich, K. (1980) *Biochem. Biophys. Res. Commun. 95*, 1−6.

Live, D. H., Davis, D. G., Agosta, W. C., & Cowburn, D. (1984) *J. Am. Chem. Soc. 106*, 1939−1941.

Lodi, P. J., Garrett, D. S., Kuszewski, J., Tsang, M. L.-S., Weatherbee, J. A., Leonard, W. J., Gronenborn, A. M., & Clore, G. M. (1994) *Science 263*, 1782−1767.

Lusti-Narasimhan, M., Power, C. A., Allet, B., Alouaai, S., Bacon, K. B., Mermod, J.-J., Proudfoot, A. E. I., & Wells, T. N. C. (1995) *J. Biol. Chem. 270*, 2716−2721.

Macura, S., Huang, Y., Suter, D., & Ernst., R. R. (1981) *J. Magn. Reson. 43*, 259−281.

Marion, D., Ikura, M., & Bax, A. (1989a) *J. Magn. Reson. 84*, 425−430.

Marion, D., Kay, L. E., Sparks, S. W., Torchia, D. A., & Bax, A. (1989b) *J. Am. Chem. Soc. 111*, 1515−1517.

Marion, D., Driscoll, P. C., Kay, L. E., Wingfield, P. T., Bax, A., Gronenborn, A. M., & Clore, G. M. (1989c) *Biochemistry 28*, 6150−6156.

Marion, D., Ikura, M., Tschudin, R., & Bax, A. (1989d) *J. Magn. Reson. 85*, 393−399.

Moser, B., Dewald, B., Barella, L., Schumacher, C., Baggiolini, M., & Clark-Lewis, I. (1993) *J. Biol. Chem. 268,* 7125−7128.
Neote, K., DiGregorio, D., Mak, J. Y., Horuk, R., & Schall T. J. (1993) *Cell 72,* 415−425.
Nilges, M. (1993) *Proteins 17,* 297−309.
Nilges, M., Clore, G. M., & Gronenborn, A. M. (1988) *FEBS Lett. 239,* 317−324.
Paolini, U. F., Willard, D., Conster, T., Luther, M., & Krangel, M. S. (1994) *J. Immunol. 153,* 2704−2717.
Pardi, A., Billeter, M., & Wüthrich, K. (1984) *J. Mol. Biol. 180,* 741−751.
Piantini, U., Sørensen O. W., & Ernst, R. R. (1982) *J. Am. Chem. Soc. 104,* 6800−6801.
Rajarthnam, K., Skyes, B. D., Kay, C. M., Dewald, B., Geiser, T., Baggioloini, M., & Clark-Lewis, I. (1994) *Science 264,* 90−92.
Rance, M. (1987) *J. Magn. Reson. 74,* 557−564.
Reilly, D., & Fairbrother, W. J. (1994) *J. Biomol. NMR 4,* 459−462.
Rucker, S. P., & Shaka, A. J. (1989) *Mol. Phys. 68,* 509−517.
Schall, T. J., Bacon, K., Toy, K. J., & Goeddel, D. V. (1990) *Nature 347,* 669−671.
Shaka, A. J., Lee, C. J., & Pines, A. (1988) *J. Magn. Reson. 77,* 274−293.
Sklenár, V., Raymond, M. P., Leppik, R., & Saudek, V. (1993) *J. Magn. Reson., Ser. A 102,* 241−245.
Sørensen, O. W., Rance, M., & Ernst, R. R. (1984) *J. Magn. Reson. 56,* 527−534.
States, D. J., Haberkorn, R. A., & Ruben, D. J. (1982) *J. Magn. Reson. 48,* 286−292.
Stonehouse, J., & Keeler, J. H. (1995) *J. Magn. Reson. Ser. A 112,* 43−57.
Studier, F. W., Rosenberg, A. H., Dunn, J. J., & Dubendorff, J. W. (1990) *Methods Enzymol. 185,* 60−89.
Tanaka, Y., Adams, D. H., Hubscher, S., Hirano, H., Sievenlist, U., & Shaw, S. (1993) *Nature 361,* 79−82.
Witanowski, M., Stefaniak, L., & Webb, G. A. (1993) *Annu. Rep. NMR Spectrosc. 25,* 167.
Wüthrich, K. (1986) *NMR of Proteins and Nucleic Acids,* John Wiley & Sons, New York.
Wüthrich K., Billetter, M., & Braun, W. (1983) *J. Mol. Biol. 169,* 947−961.
Zhang, X., Chen, L., Bancroft, D. P., Lai, C. K., & Maione, T. E. (1994) *Biochemistry 33,* 8361−8366.

BI950650T